INTERNATIONAL JOURNAL FOR NUMERICAL METHODS IN ENGINEERING
Int. J. Numer. Meth. Engng 0000; **00**:1–15
Published online in Wiley InterScience (www.interscience.wiley.com). DOI: 10.1002/nme

Novel basis functions for the partition of unity boundary element method for Helmholtz problems

M. J. Peake*, J. Trevelyan and G. Coates

School of Engineering and Computing Sciences, Durham University, South Road, Durham, DH1 3LE, UK

SUMMARY

The boundary element method (BEM) is a popular technique for wave scattering problems given its inherent ability to deal with infinite domains. Recently, the partition of unity BEM, in which the approximation space is enriched with a linear combination of plane waves, has been developed; this significantly reduces the number of degrees of freedom required per wavelength. It has been shown that the element ends are more susceptible to errors in the approximation than the mid-element regions. In this paper the authors propose that this is due to the reduced order of continuity in the Lagrangian shape function component of the basis functions. It is demonstrated, using numerical examples, that choosing trigonometric shapes functions, rather than classical quadratic shape functions, provides accuracy benefits. It is also demonstrated that the somewhat arbitrary choice of collocating at equally spaced points about the surface of a scatterer is, in fact, the optimum choice of collocation scheme. Copyright © 0000 John Wiley & Sons, Ltd.

Received . . .

KEY WORDS: boundary element method; partition of unity; collocation

1. INTRODUCTION

The finite element method (FEM) and boundary element method (BEM) have become well-established techniques for finding solutions to a wide range of engineering problems. This paper deals with the solution of frequency-domain, boundary-value problems in wave propagation and scattering. The BEM is well suited to problems of this type; in particular, problems set in infinite domains. The more prevalent FEM requires such domains to be truncated and, to approximate infinity, artificial boundary conditions to be set; in contrast, the BEM automatically satisfies boundary conditions at infinity and no domain truncation is required.

The BEM was first used to solve the Helmholtz by Banaugh and Goldsmith [1] who derived the boundary integral equation (BIE) using Green's second identity; the authors' derivation of the boundary integral for acoustics does not differ greatly from Banaugh and Goldsmith's approach. Copley [2] noted that the BIE formulation suffered from a problem of nonuniqueness at discrete eigenfrequencies associated with the interior Dirichlet problem. Copley showed that a method collocating only at internal points would provide a unique solution for all problems, though it was less numerically stable. Schenck [3] overcame the nonuniqueness by using a combination of the classical BEM method with Copley's internal points known as the Combined Helmholtz Integral Equation Formulation (CHIEF). Other popular solutions to the nonuniqueness problem include the Burton and Miller approach [4].

*Correspondence to: School of Engineering and Computing Sciences, Durham University, South Road, Durham, DH1 3LE, UK. E-mail: m.j.peake@durham.ac.uk

Contract/grant sponsor: EPSRC

Conventional BEM schemes require the mesh to be refined as the wavelength, λ, of the problem decreases. Using a conventional, polynomial, shape function basis, there is a well-known heuristic rule that prescribes a minimum of 10 degrees of freedom per wavelength in each coordinate direction in order to obtain an 'engineering accuracy' ($\sim 1\%$). This is not unique to the BEM and similar restrictions are found using the finite element and meshless methods. In effect, this places an upper limit on the frequency that may be considered for a problem given a specific computational resource. Much research over the last decade has been focused on increasing this limit.

In a theme issue of *Philosophical Transactions of the Royal Society A*, Bettess [5] provided a review of the problem of shortwaves—"waves in which the wavelength is much smaller than any other parameters in the problem"—and the techniques developed to address these. Readers are directed to this theme issue for more details on some of the approaches.

Abboud *et al.* [6] showed that, for a convex scatterer of size much greater than λ, the scattered potential may be approximated as the product of a slowly varying function and the incident wave impinging the scatterer. This varying function can then be obtained by approximating it about the boundary of the scatterer using a boundary element scheme. Bruno *et al.* [7] have shown the complexity of this approach to be independent of the wavenumber, presenting results for scatterers of dimension $10^6\lambda$; Langdon and Chandler-Wilde [8] have shown that this approach is suitable for polygonal scatterers; Domínguez *et al.* [9] demonstrated that, to maintain a fixed error bound for problems of asymptotically large wavenumbers, the required number of degrees of freedom increases only with $\mathcal{O}k^{1/9}$; Anand *et al.* [10] have extended the approach for problems of multiple scatterers.

An extension of these ideas to consider a basis with multiple plane waves, for an integral equation approach, was introduced by de la Bourdonnaye [11]. The Partition of Unity Method (PUM), introduced by Bubuška and Melenk [12], generalised the approach of using approximation spaces enriched by a set of functions known to populate the solution space for any differential equation under consideration; for wave problems, sets of plane waves were proposed. This approach was applied to the FEM by Laghrouche *et al.* [13]. The parition of unity FEM (PUFEM) can also be seen in the ultra weak variational formulation [14, 15], the discontinuous enrichment method [16], and the Variational Theory of Complex Rays [17, 18].

In boundary elements, the PUM has been applied to the Galerkin BEM by Bériot *et al.* [19] and to the collocation BEM by Perrey-Debain *et al.* [20]. Perrey-Debain *et al.* showed that the partition of unity boundary element method (PU-BEM) requires approximately 3 degrees of freedom per wavelength, a marked reduction on the 10 prescribed for piecewise polynomial approximations.

Trevelyan and Coates [21] presented an adaptive basis for the collocation PU-BEM. They noted that residual errors are largest at the ends of elements. It was suggested that this was due to the lack of continuity in the quadratic shape functions used. This paper will introduce a novel set of shape functions that provide greater continuity between elements and, thus, reduce these residual errors.

2. PARTITION OF UNITY BOUNDARY ELEMENT METHOD FOR THE HELMHOLTZ EQUATION

2.1. Formulation of the Helmholtz boundary integral equation

Let $\Omega \subset \mathbb{R}^2$ be a domain, with no exterior boundary and with a smooth internal scatterer of boundary $\partial\Omega = \Gamma$. Assuming time dependence, the wave equation can be reduced to the Helmholtz equation,

$$\nabla^2\phi(\mathbf{P}) + k^2\phi(\mathbf{P}) = 0, \quad \phi \in \mathbb{C}, \mathbf{P} \in \Omega, \tag{1}$$

where ∇^2 is the Laplacian operator, $\phi(\mathbf{P})$ is the unknown potential field at $\mathbf{P}$, and $k = 2\pi/\lambda$ is the wavenumber (λ is the wavelength).

Let the scatterer be impinged by an incident plane wave,

$$\phi^{\mathrm{I}}(\mathbf{P}) = A^{\mathrm{I}} \exp(ik\,\mathbf{d}^{\mathrm{I}} \cdot \mathbf{P}), \tag{2}$$

where A^{I} is the plane wave amplitude and $\mathbf{d}^{\mathrm{I}}$ is a unit-vector pointing in the direction of propagation.

DOI: 10.1002/nme

Obtaining the boundary integral equation (BIE) from (1) using Green's second identity is well known [22] and yields

$$c(\mathbf{p})\phi(\mathbf{p}) = \int_\Gamma \frac{\partial\phi(\mathbf{q})}{\partial n} G(\mathbf{p},\mathbf{q})\,\mathrm{d}\Gamma_\mathbf{q} - \int_\Gamma \phi(\mathbf{q})\frac{\partial G(\mathbf{p},\mathbf{q})}{\partial n}\,\mathrm{d}\Gamma_\mathbf{q} + \phi^\mathrm{I}(\mathbf{p}), \quad \mathbf{p},\mathbf{q}\in\Gamma, \tag{3}$$

where n is the outward-pointing, unit normal at the integration point $\mathbf{q}$ and, assuming the boundary is smooth, $c(\mathbf{p}) = 1/2$ at the evaluation point $\mathbf{p}$. Further, $G(\mathbf{p},\mathbf{q})$ is the fundamental solution (Green's function), representing the effect experienced at $\mathbf{q}$ due to a unit source radiating at $\mathbf{p}$ (or *vice versa*). In two-dimensional space, it is a cylindrical wave, given by

$$G(\mathbf{p},\mathbf{q}) = \frac{i}{4}H_0^{(1)}(kr), \tag{4}$$

where $H_0^{(1)}(\cdot)$ is a Hankel function of the first kind, order 0, and $r := |\mathbf{p}-\mathbf{q}|$.

A solution to (1) is sought, subject to a general Robin boundary condition,

$$\frac{\partial\phi(\mathbf{q})}{\partial n} = \beta(\mathbf{q})\phi(\mathbf{q}) + g(\mathbf{q}) \tag{5}$$

so that (3) may be reformulated as

$$c(\mathbf{p})\phi(\mathbf{p}) + \int_\Gamma \left[\frac{\partial G(\mathbf{p},\mathbf{q})}{\partial n} - G(\mathbf{p},\mathbf{q})\beta(\mathbf{q})\right]\phi(\mathbf{q})\,\mathrm{d}\Gamma_\mathbf{q} = \int_\Gamma G(\mathbf{p},\mathbf{q})g(\mathbf{q}),\mathrm{d}\Gamma_\mathbf{q} + \phi^\mathrm{I}(\mathbf{p}). \tag{6}$$

g is zero for passive boundary conditions and non-zero for active boundary conditions (radiation problems). This approach is applicable for sound-soft and impedance boundary conditions; however, for a compact presentation, the case of a perfectly reflecting ("sound-hard") scatterer is considered i.e. $\beta(\mathbf{p}) = g(\mathbf{p}) = 0$ and (6) is rewritten in the form

$$c(\mathbf{p})\phi(\mathbf{p}) + \int_\Gamma \frac{\partial G(\mathbf{p},\mathbf{q})}{\partial n}\phi(\mathbf{q})\,\mathrm{d}\Gamma_\mathbf{q} = \phi^\mathrm{I}(\mathbf{p}). \tag{7}$$

2.2. Direct collocation BEM

In the classical, direct collocation BEM, Γ is discretised into E elements, such that

$$\Gamma = \bigcup_{e=1}^{E}\Gamma_e \quad \text{and} \quad \Gamma_e\bigcap\Gamma_j = \emptyset, \quad e\neq j. \tag{8}$$

Each element geometry is analytical and given by

$$\Gamma_e = \{\gamma_e(\xi) : \xi\in[-1,1]\}, \tag{9}$$

where $\gamma_e : \mathbb{R}\to\mathbb{R}^2$. For any element, the mapping between $\mathbf{q}\in\Gamma$ and ξ is unique and bidirectional, hence it shall be assumed, from hereon, that any function $f(\mathbf{q})$ is equivalent to $f(\xi)$. The variation of potential on element e can be formally expressed in a piecewise polynomial basis

$$\phi^e(\mathbf{q}) = \sum_{j=1}^{J} N_j(\xi)\phi_j^e, \tag{10}$$

where J is the number of nodes on the element (and order of the variation), and N_j and ϕ_j^e are the shape function and unknown potential, respectively, for node j. Substitution of (10) into (7) results in the reformulated BIE,

$$c(\mathbf{p})\phi(\mathbf{p}) + \sum_{e=1}^{E}\sum_{j=1}^{J}\int_{-1}^{+1}\frac{\partial G(\mathbf{p},\mathbf{q})}{\partial n}N_j(\xi)J^t(\xi)\,\mathrm{d}\xi\,\phi_j^e = \phi^\mathrm{I}(\mathbf{p}), \tag{11}$$

where J^t is the Jacobian of the mapping in (9). The integrals within (11) can be evaluated using quadrature, taking care to use an appropriate scheme (e.g. [23, 24]) when considering the singular integrals that arise.

To find the potential on Γ, (11) is collocated at each of the element nodes to yield a system of linear equations that can be solved in a conventional fashion.

DOI: 10.1002/nme

2.3. Partition of Unity BEM

To move from the the classical, direct collocation BEM to the PU-BEM, a plane wave expansion of the potential on element e is introduced such that (10) is replace by

$$\phi^e(\mathbf{q}) = \sum_{j=1}^{J} N_j(\xi) \sum_{m=1}^{M} A^e_{jm} \exp\left(ik\,\mathbf{d}^e_{jm}\cdot\mathbf{q}\right), \quad \left|\mathbf{d}^e_{jm}\right| = 1, \tag{12}$$

where M is the number of plane waves in the expansion per node and, respectively, $\mathbf{d}^e_{jm} \in \mathbb{R}^2$ and $A^e_{jm} \in \mathbb{C}$ are the prescribed directions and unknown amplitudes of the plane waves in the basis. As with the classical direct collocation BEM, degrees of freedom at nodes that are shared by adjacent elements are considered to have the same value for each element; thus, C^0 continuity in potential across element interfaces is obtained.

Substitution of (12) into (7) gives

$$c(\mathbf{p})\phi(\mathbf{p}) + \sum_{e=1}^{E}\sum_{j=1}^{J}\sum_{m=1}^{M}\int_{-1}^{+1} \frac{\partial G(\mathbf{p},\mathbf{q})}{\partial n} N_j(\xi)\exp(ik\,\mathbf{d}^e_{jm}\cdot\mathbf{q}) J^t(\xi)\,\mathrm{d}\xi\, A^e_{jm} = \phi^{\mathrm{I}}(\mathbf{p}). \tag{13}$$

This discretised form the of the BIE for the PU-BEM can be collocated, similar to before.

M may be chosen such that a requirement of the number of degrees of freedom per wavelength, τ, is obtained, locally and globally. For FEM and BEM approximations, $\tau \geq 10$ is, generally, required; however, it has been shown that, for PU-BEM, $\tau \simeq 3$ is sufficient for an accuracy $\sim 1\%$ [20]. Further, it is observed that τ may be reduced towards 2.0 as k increases and may become considerably smaller for convex scatterers when k is large. In this paper, the authors consider the more challenging problem of a moderate k. In most PU-BEM literature, the plane wave directions are defined to be equally distributed around the unit circle, i.e.

$$\mathbf{d}^e_{jm} = \left(\cos\theta^e_{jm}, \sin\theta^e_{jm}\right), \quad \theta^e_{jm} = \frac{2\pi(m-1)}{M} + \theta^{\mathrm{I}}, \tag{14}$$

where θ^{I} is the angle of incidence of the incident plane wave, ϕ^{I}. Since, for asymptotically large k, the potential ϕ in the illuminated zone takes a value of $2\phi^{\mathrm{I}}$, it is common to include the incident wave direction in the approximation basis.

There are, then, M degrees of freedom associated with each node so collocation at each node does not provide a sufficient number of equations with which to solve the system. More equations are provided by collocating at a sufficient number of points over the boundary. This requires that the potential at each collocation point, $\phi(\mathbf{p})$, to be expanded in a similar fashion to (12), thus

$$\phi(\mathbf{p}) = \sum_{j=1}^{J} N_j(\mathbf{p}) \sum_{m=1}^{M} A^{\bar{e}}_{jm} \exp(ik\,\mathbf{d}^{\bar{e}}_{jm}\cdot\mathbf{p}), \tag{15}$$

where $\bar{e}$ is the element on which $\mathbf{p}$ lies.

Collocation yields a square system of equations,

$$[(1/2)\mathbf{C} + \mathbf{H}]\{\mathbf{x}\} = \{\mathbf{b}\}, \tag{16}$$

where the sparse, square matrix $\mathbf{C}$ results from interpolations of the plane waves through (15) and the square matrix $\mathbf{H}$ is fully populated with the boundary integrals contained in (13). The right-hand side vector $\{\mathbf{b}\}$ contains the incident wave potentials, at the collocation points, defined in (2), and the unknown vector $\{\mathbf{x}\}$ contains the amplitudes, A^e_{jm}.

2.4. Nonuniqueness

With this formulation, and the classical boundary collocation BEM, a method needs to be employed to overcome the problem of nonuniqueness of the solution to (7) at the eigenfrequencies of the

DOI: 10.1002/nme

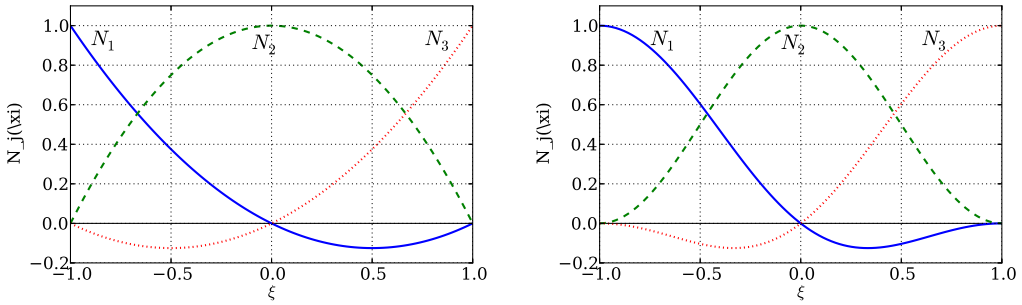

(a) Quadratic shape functions

(b) Trigonometric shape functions

Figure 1. Comparison of shape functions with partition of unity

associated interior Dirichlet problem. The current authors use the CHIEF approach [3] for reasons of computational efficiency.

The CHIEF approach requires collocation at, in addition to the boundary collocation points, a number of interior coordinates. These yield a set of equations which can be appended to (16). The system of equations now becomes

$$\begin{bmatrix} \frac{1}{2}\mathbf{C} + \mathbf{H} \\ \mathbf{H}_{\mathrm{CHIEF}} \end{bmatrix} \{\mathbf{x}\} = \begin{Bmatrix} \mathbf{b} \\ \mathbf{b}_{\mathrm{CHIEF}} \end{Bmatrix}, \tag{17}$$

where $\mathbf{H}_{\mathrm{CHIEF}}$ is populated with boundary integrals evaluated from an adapted version of (13) for collocation points outside the solution domain:

$$\sum_{e=1}^{E} \sum_{j=1}^{J} \sum_{m=1}^{M} \int_{-1}^{+1} \frac{\partial G(\mathbf{p},\mathbf{q})}{\partial n} N_j(\xi) \exp(ik\, \mathbf{d}^e_{jm} \cdot \mathbf{q}) J^t(\xi)\, \mathrm{d}\xi\, A^e_{jm} = \phi^{\mathrm{I}}(\mathbf{p}), \quad \mathbf{p} \notin \Omega, \mathbf{q} \in \Gamma. \tag{18}$$

$\mathbf{b}_{\mathrm{CHIEF}}$ is evaluated from (2). This is system is rectangular and, generally, ill-conditioned; in order to solve it for $\mathbf{x}$ accurately, the current authors use Singular Value Decomposition (SVD). A more cost effective solution would be to develop a bespoke preconditioner for PU-BEM systems; this is a subject for further research.

3. TRIGONOMETRIC SHAPE FUNCTIONS

Polynomial shape functions have been commonly used in the both the FEM and BEM since the 1980s [25, 26]; however, no study of shape functions has been carried out for the PU-BEM. It has been previously noted [21] that errors in the PU-BEM are greatest at the end of the boundary elements. A likely source of these errors is the C^0 nature of quadratic shape functions. Figure 1a shows the classical quadratic shape functions expressed by

$$N_1(\xi) = \frac{1}{2}\xi(\xi - 1), \quad N_2(\xi) = (1 + \xi)(1 - \xi), \quad N_3(\xi) = \frac{1}{2}\xi(\xi + 1). \tag{19}$$

Each of the shape functions has non-zero gradient at the element ends; this produces a discontinuity, in the first derivative, between adjoining elements. Increasing the continuity between elements, in order to reduce these errors, is the principal aim of the current work.

To design some continuous shape functions with the partition of unity property, the following rules must be obeyed:

- $N_j(\xi) = 1$ at the node j,
- $N_j(\xi) = 0$ at all other nodes,
- $\sum N_j(\xi) = 1 \quad \forall\, \xi.$

(20)

DOI: 10.1002/nme

Trigonometric functions have well known smoothness and C^∞ continuity. It can be assumed that there is a set of shape functions of the form

$$\begin{aligned} N_1(\xi) &= \alpha_1 \cos(\pi\xi) + \alpha_2 \sin\left(\frac{\pi}{2}\xi\right) + \alpha_3, \\ N_2(\xi) &= \alpha_4 \cos(\pi\xi) + \alpha_5 \sin\left(\frac{\pi}{2}\xi\right) + \alpha_6, \\ N_3(\xi) &= \alpha_7 \cos(\pi\xi) + \alpha_8 \sin\left(\frac{\pi}{2}\xi\right) + \alpha_9. \end{aligned} \tag{21}$$

Then, using the rules in (20), three sets of three simultaneous equations are obtained. When solved, it is found that the shape functions are

$$\begin{aligned} N_1(\xi) &= -\frac{1}{4}\cos(\pi\xi) - \frac{1}{2}\sin\left(\frac{\pi}{2}\xi\right) + \frac{1}{4}, \\ N_2(\xi) &= \frac{1}{2}\cos(\pi\xi) + \frac{1}{2}, \\ N_3(\xi) &= -\frac{1}{4}\cos(\pi\xi) + \frac{1}{2}\sin\left(\frac{\pi}{2}\xi\right) + \frac{1}{4}. \end{aligned} \tag{22}$$

These shape functions can be seen in Figure 1b. They have zero gradient at the element ends; partition of unity can be easily proved by summing the three shape functions. The following section provides some numerical results examining the effectiveness of using trigonometric shape functions.

4. NUMERICAL RESULTS WITH TRIGONOMETRIC SHAPE FUNCTIONS

The new trigonometric shape functions (22) can be used for a range of problems solved using the PU-BEM. In the following examples, the sound-hard boundary condition is used. Errors, $\mathcal{E}$, are evaluated using L_2-norms:

$$\mathcal{E} = \frac{\|\Phi - \Phi^{\mathrm{ex}}\|_{L_2}}{\|\Phi^{\mathrm{ex}}\|_{L_2}}, \tag{23}$$

where Φ is a vector of potentials, evaluated using the PU-BEM, on the surface of the scatterer and Φ^{ex} is a vector of exact potentials evaluated analytically or by a converged solution.

4.1. Scattering by a circular cylinder

Consider a cylindrical scatterer of radius $a = 1$, centred at $(0, 0)$; the scatterer is impinged by a unit-amplitude, incident plane wave propagating in the direction $(1, 0)$. The analytical solution for the total field, at any point $\mathbf{q}$, on the surface of the cylinder can be expressed by the following, adapted from [27],

$$\phi(\mathbf{q}) = \frac{2}{\pi k a} \sum_{n=0}^{\infty} \varepsilon_n \frac{i^{n+1}}{H_n'(ka)} \cos(n\theta), \tag{24}$$

where $\mathbf{q} = a(\cos\theta, \sin\theta)$, ε_n denotes the Neumann symbol ($\varepsilon_0 = 1$; $\varepsilon_n = 2$ for $n = 1, 2, 3, ...$) and $H_n'(ka)$ denotes the derivative of $H_n(ka)$ with respect to ka.

The quality of the solution Φ for a range of k is investigated. As the wavenumber is increased, M is increased to maintain $\tau = 2ME\lambda/P \approx 3$, where P is the length of Γ and E is the number of elements.

Two sets of errors (boundary representation by two elements and four elements) are displayed in Figure 2. Results for a conventional (i.e. piecewise quadratic with $\tau \approx 10$) BEM have been included to demonstrate the benefits of using the PU-BEM. The results for PU-BEM simulations are not only more accurate by orders of magnitude; they also require far less memory and computational effort due to a significantly reduced τ. For two-dimensional problems (and excluding CHIEF points), the size of the system matrix is directly proportional to τ^2; thus, the PU-BEM system is approximately 90% smaller than the conventional BEM system matrix. In spite of the increased requirement to

Prepared using nmeauth.cls
DOI: 10.1002/nme

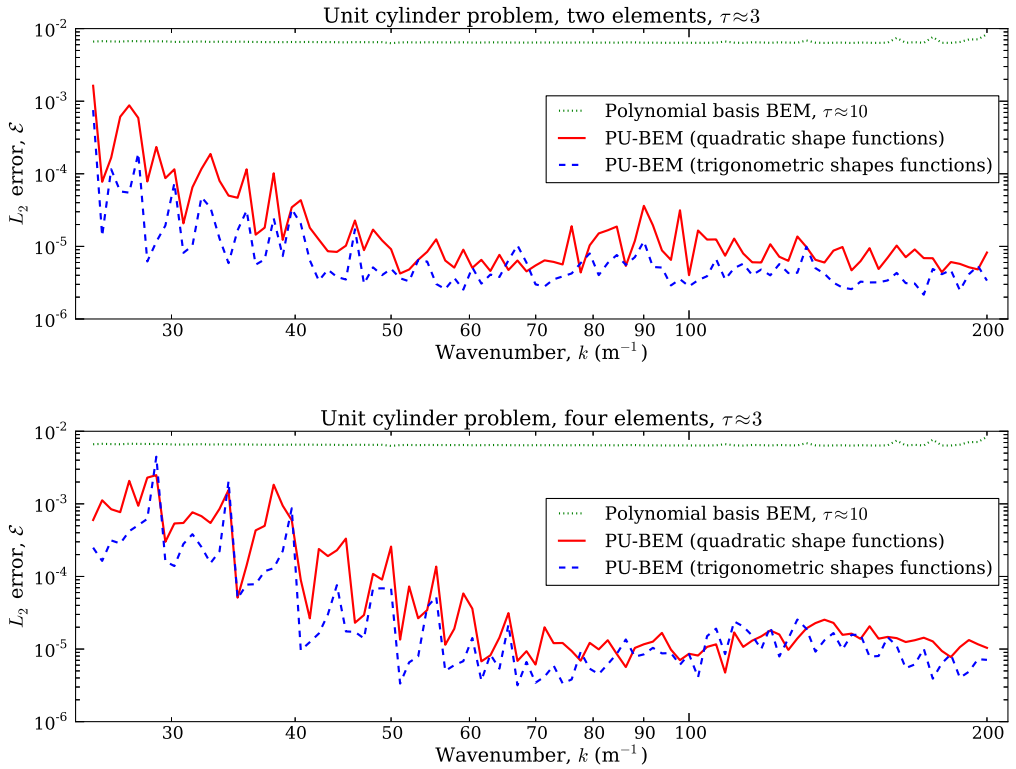

Figure 2. Error analysis for the hard, unit-radius, circular cylinder problem: $\mathbf{d}^{\mathrm{I}} = (1, 0)$

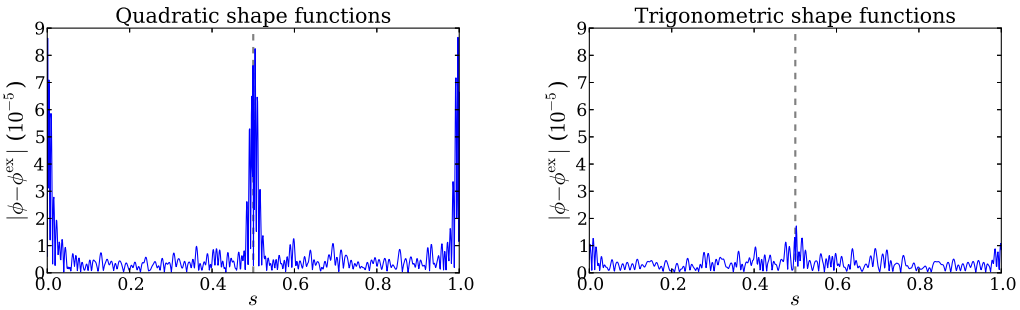

Figure 3. Plots of absolute difference between PU-BEM and analytical solution for circular cylinder problem, $k = 50$

evaluation of highly oscillatory integrals, the run time for PU-BEM models was, typically, only 5 to 20% of that required for the piecewise quadratic BEM approximation.

As k varies, the integer M is varied to keep $\tau \approx 3$. This produces large changes in τ, particularly for smaller k; this leads to the oscillating errors of the PU-BEM. Figure 2 displays clearly that the trigonometric shapes functions provide an accuracy benefit; however, a plot of errors over the surface of the cylinder is required to demonstrate where these accuracy improvements originate.

Figure 3 shows a comparison of the errors arising from each type of shape function. The coordinate $s \in [0, 1]$ runs clockwise around the cylinder, starting at the cartesian coordinate $(1, 0)$; the dashed line represents an element end. Using quadratic shape functions, the error peaks are greater at the end of the the two elements. Using the trigonometric shape functions has significantly reduced the magnitude of the errors in this region; the maximum error is reduced by 80%.

DOI: 10.1002/nme

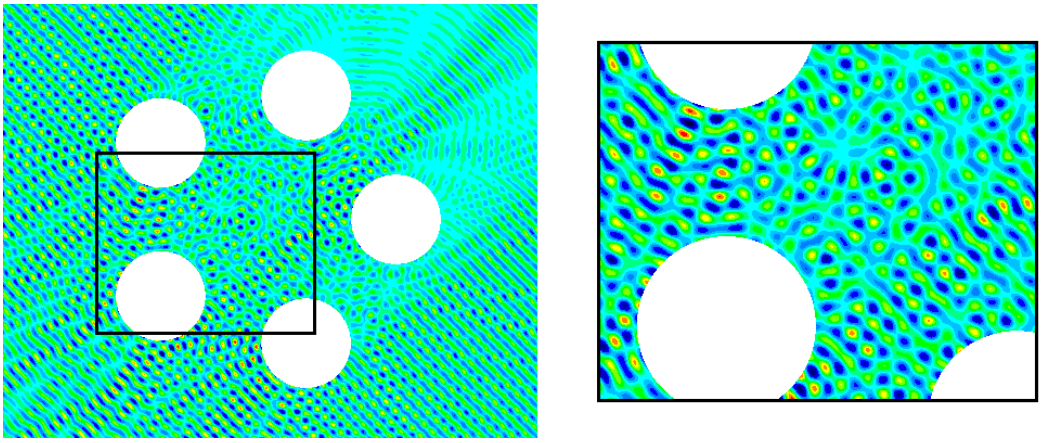

Figure 4. Illustration of the internal reflections caused by the five-cylinder geometry: $\lambda = 0.25$

4.2. Scattering by five circular cylinders

Consider a set of cylindrical scatters impinged by an incident plane wave. An analytical solution for this problem, in the form of an infinite series, was presented by Linton and Evans [28]; the solution is valid for any cylinder radii and location, provided the cylinders do not overlap or touch. Linton and Evans show that, for a set of N cylinders, the velocity potential on the vth cylinder can be expressed as

$$\phi\left(a_v, \theta_v\right) = -\frac{2i}{\pi k a_v} \sum_{n=-\infty}^{\infty} \frac{A_n^v}{H_n'(ka_v)} e^{in\theta_v}, \tag{25}$$

where A_n^v are constants that are found by using the equation

$$A_m^v + \sum_{\substack{u=1 \\ \neq v}} \sum_{n=-M}^{M} A_n^u Z_n^u e^{i(n-m)\alpha_{uv}} H_{n-m}\left(kR_{uv}\right) = -I_v e^{im\left(\pi/2-\theta^{\mathrm{I}}\right)}, \qquad v = 1, \ldots, N, \quad m = -\infty, \ldots, \infty, \tag{26}$$

where α_{uv} and R_{uv} are the angle and distance between the centres of the uth and vth cylinder; I_v is a phase factor associated with the vth cylinder and

$$Z_n^u (\equiv Z_{-n}^u) = H_n(kr_u), \tag{27}$$

where r_u is the distances between the origin and the centre of the uth cylinder. (26) is truncated so that $m = -M, \ldots, M$ and a square system of $N(2M+1)$ can be solved. Increasing M improves the accuracy of the constants at the expense of computing time.

The problem presented here is that of five cylinders, of unit-radius, with centres distributed, equally, $r = 3$ from the origin, i.e. at the polar coordinates $(3, 2n\pi/5)$ for $n = 0, 1, 2, 3, 4$. This geometry is chosen as it creates internal reflections between the cylinders; this can be seen, for $\lambda = 0.25$, in Figure 4.

Similarly to the single cylinder case, PU-BEM simulations were run, using quadratic and trigonometric shapes functions, using two different meshes: boundary representation with two elements and four elements. The parameter τ was approximately 3 for all simulations. Results are displayed in Figure 5.

It is clear, again, that the trigonometric shape functions, due to the increased continuity between elements, provide an accuracy benefit for the majority of the simulations.

DOI: 10.1002/nme

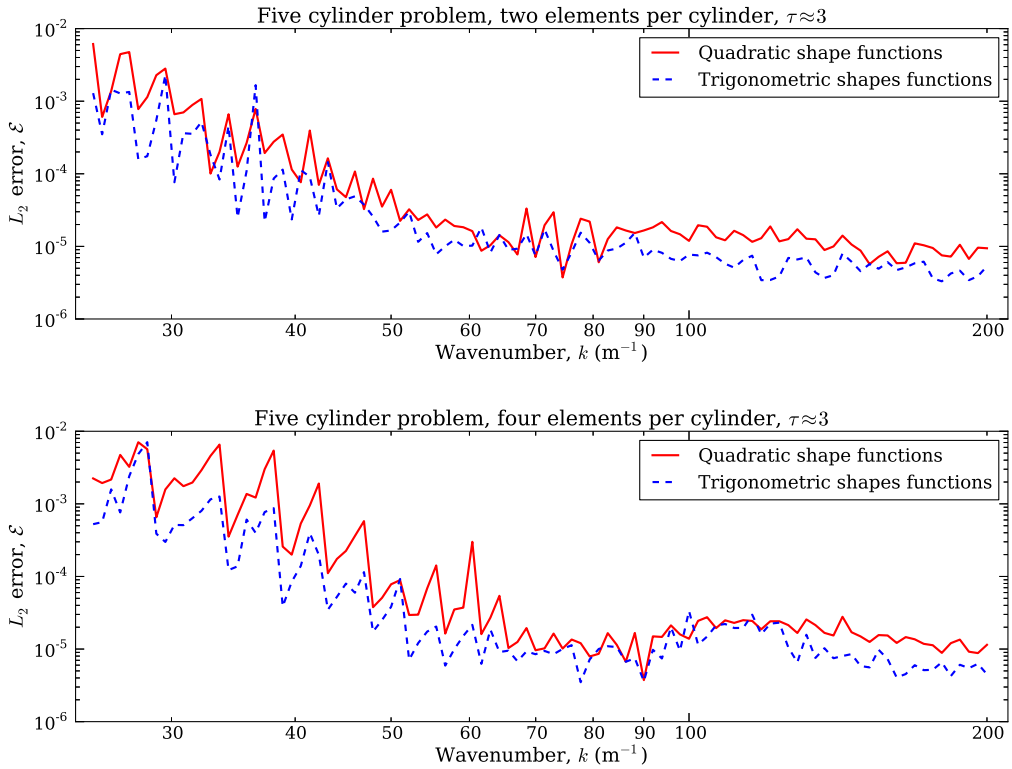

Figure 5. Error analysis for the hard, unit-radius, circular cylinders problem: $\mathbf{d}^{\mathrm{I}} = (0.707, 0.707)$

4.3. Scattering by a capsule

An area of interest is the blending point between different types of geometry component, e.g. a line and an arc; since this presents a geometry with only C^1 continuity, these regions are susceptible to errors. To investigate the ability of trigonometric shape functions to capture accurately the solution over C^1 boundaries, a capsule shape was designed consisting of two semi-circular arcs (unit-radius) and two lines.

Figure 6 displays the capsule geometry discretised by three elements of equal length. The element ends, at $s = 0, 1/3, 2/3$, are represented by lines across the boundary. The coordinates show the origin, arc centres and blend points between lines and arcs. Elements of equal length make the trigonometric shape functions provide the greatest continuity; this provides the best approximation of potential along the surface of the scatterer. As geometry points are taken analytically, this does not impact the evaluation of the integral kernels.

Similar to the previous test cases, PU-BEM simulations were run, using quadratic and trigonometric shapes functions. The parameter τ was approximately 3 for all simulations. There is no analytical solution for this problem so a converged solution using the method of fundamental solutions (MFS) [29] was used as an exact solution.

Figure 7 shows the errors, $\mathcal{E}$, over a range of wavenumbers. The trigonometric shape functions produce accuracy benefits at lower wavenumbers; however, at higher wavenumbers, the benefits are reduced. The current authors suggest that this is because, at high wavenumbers, there are a large number of plane waves in the expansion which become the most dominant part of the basis. For example, consider the capsule problem and unit-cylinder problem for $k = 100$. The potential on each node in the unit-cylinder problem is expanded as a linear combination of 63 plane waves; for the capsule problem, the potential at each node is expanded as a linear combination of 82

DOI: 10.1002/nme

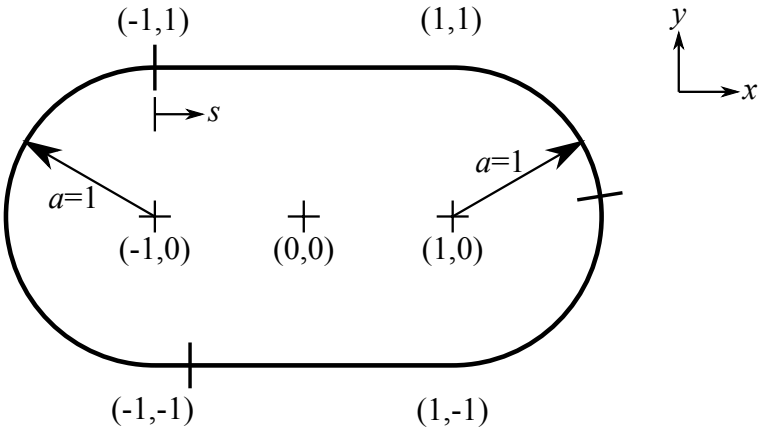

Figure 6. Capsule discretised by three equal-length elements

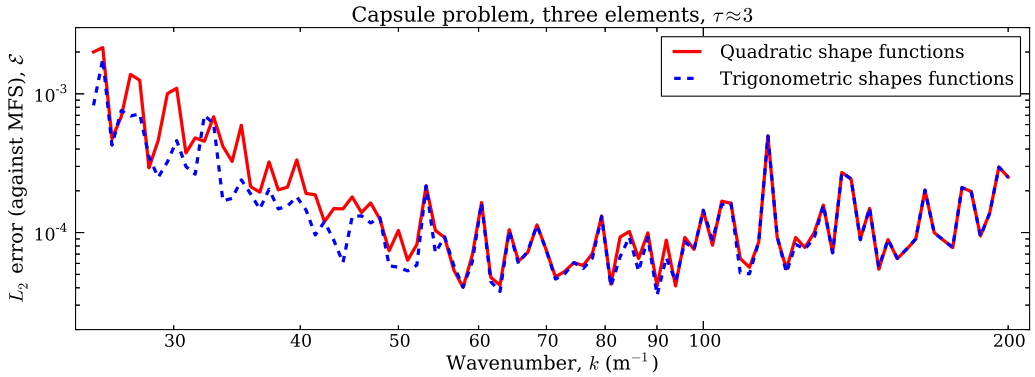

Figure 7. Error analysis for the hard capsule problem: $\mathbf{d}^{\mathrm{I}} = (0.5, \sqrt{3}/2)$

plane waves. With 30% more plane waves in each expansion, these dominate the enrichment for the capsule problem and reduce the observable effect of using trigonometric shape functions.

Figure 8 shows the absolute difference, along the surface of the scatterer, between the PU-BEM solution and the converged MFS solution. As before, there are significant errors at the element ends that are reduced by the trigonometric shape functions; the maximum error is reduced by 60%. There are also significant errors at the blend points between the lines and arcs; these errors have been reduced but are still large in comparison to the errors over the rest of the boundary. Clearly, the trigonometric shape functions, though continuous through these points, are not sufficient to describe, ideally, the C^1 geometry's effect on the potential in those areas.

4.4. Time to run simulations

It may be expected that the computational resources required to evaluate the trigonometric shape functions would exceed those required to compute the corresponding quadratic shape functions. Modern processors and programming packages, however, have significantly reduced this computational burden. Also, the computational time of the PU-BEM is dominated by the calculation of the Hankel functions rather than shape functions. Table I compares some normalised times of simulations run for the capsule problems for a selection of wavenumbers. The trigonometric shape functions clearly do not increase the time taken to run a simulation; indeed, they appear to slightly reduce the time. It is evident, therefore, that the introduction of trigonometric shapes functions does not induce a computational burden.

DOI: 10.1002/nme

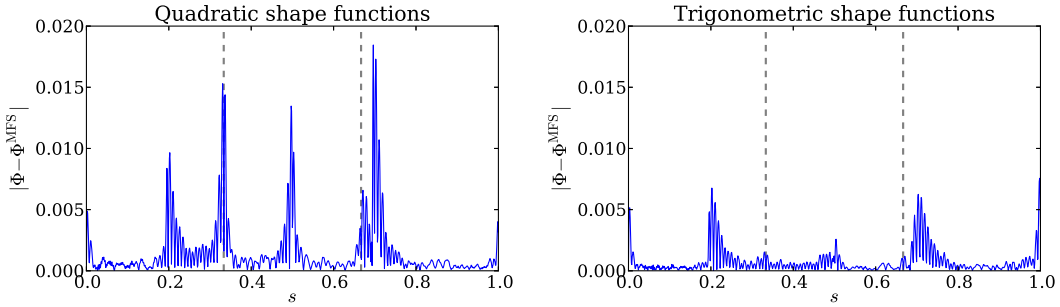

Figure 8. Plots of absolute difference of PU-BEM against converged MFS solution for capsule problem, $k = 25$

Table I. Comparison of simulation times using quadratic and trigonometric shape functions

	System build (s/8.675)	System solve (s/7.429)
k=30, Quadratic	0.042	0.015
k=30, Trigonometric	0.041	0.015
k=70, Quadratic	0.206	0.135
k=70, Trigonometric	0.206	0.133
k=150, Quadratic	1.000	1.000
k=150, Trigonometric	0.988	0.997

5. ALTERNATIVE COLLOCATION STRATEGIES

To the authors' knowledge, the choice of collocation strategy with the PU-BEM is somewhat arbitrary and has not been formally investigated. For a polynomial basis BEM, it is sufficient to collocate the boundary integral at each element node; for the PU-BEM, the boundary integral has, generally, been collocated at a sufficient number of equally spaced points on the boundary. In adaptive basis schemes, such as [21], additional collocation points are added between existing collocation points; however, the current authors consider only an initial array of collocation points.

The motivation for this part of the work is to investigate and reduce errors that may be associated with the collocation strategy. In view of the fact that the work considers frequency domain wave scattering, where waves can be modelled as sine curves, uniformly spaced collocation points have the potential to act like a digital filter.

Three alternative approaches to the choice of collocation points are suggested here. In all cases, the sound-hard cylinder problem (Section 4.1) is used as the test case; the results for trigonometric shape functions are displayed.

5.1. Collocating using roots of polynomials

When examining the absolute error plots (Figures 3 and 8), it can be seen that the the errors approach zero at a number of points along each element; these points correspond with the collocation points on each element. If collocation points are clustered towards on area on an element, this reduces the absolute errors in that region. Applying this approach, clustering collocation points towards the ends of elements, is one way to reduce errors at the element ends; however, this will, subsequently, increase errors at regions of less clustered collocation points.

One way in which to produce a 'clustered' collocation scheme is to use the roots of classical orthogonal polynomials. Here, the authors provide results for three, well-known polynomials: Chebyshev and Legendre (both special types of Jacobi polynomial), and Hermite polynomial. In each case, a number of roots can be found which can then be mapped onto the local coordinate

DOI: 10.1002/nme

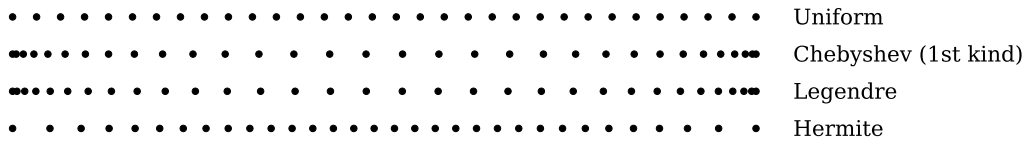

Figure 9. Uniform, Chebyshev, Legendre and Hermite collocation points in $[-1, 1]$ for 32 collocation points

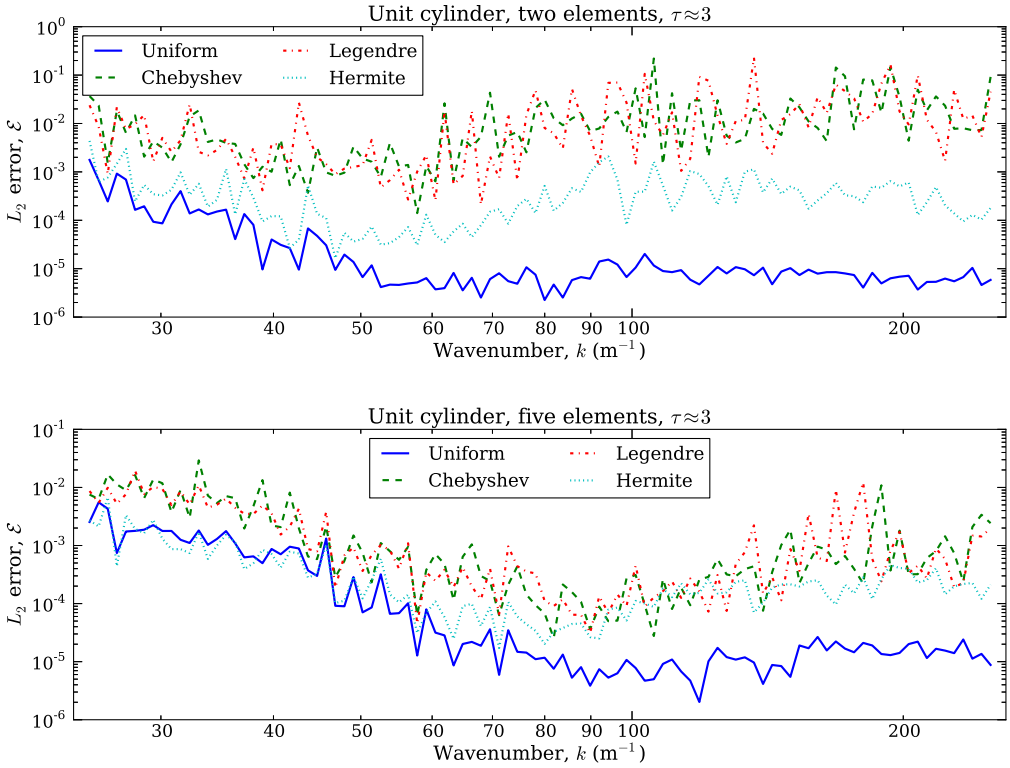

Figure 10. Comparison of collocation strategies based on polynomial roots

$\xi \in [-1, 1]$; collocation can be guaranteed at $\xi = \pm 1$. Figure 9 shows how the collocation schemes differ for a specific number of collocation points.

Figure 10 shows the errors, $\mathcal{E}$, when these polynomials were used as the collocation scheme for the unit cylinder problem, over a range of wavelengths. It is clear that none of the above collocation schemes are effective at improving the accuracy of the solution. The uniform spacing provides a greater accuracy. Compared to the Chebyshev and Legendre schemes (clustering collocation towards the elements ends), the uniform spacing provided an accuracy benefit between one and four orders of magnitude in most cases. Indeed, the best alternative scheme to uniformly spaced collocation points was the Hermite roots.

5.2. Consideration of the Fock domain

Consider a cylinder approximated by four, equal-length elements. If one element faces the impinging wave, it is said to be in the illuminated zone; the element on the opposite side of the cylinder is in the shadow zone. The remaining two elements, that lie between the illuminated and shadow zone, are said to be in the Fock domain.

DOI: 10.1002/nme

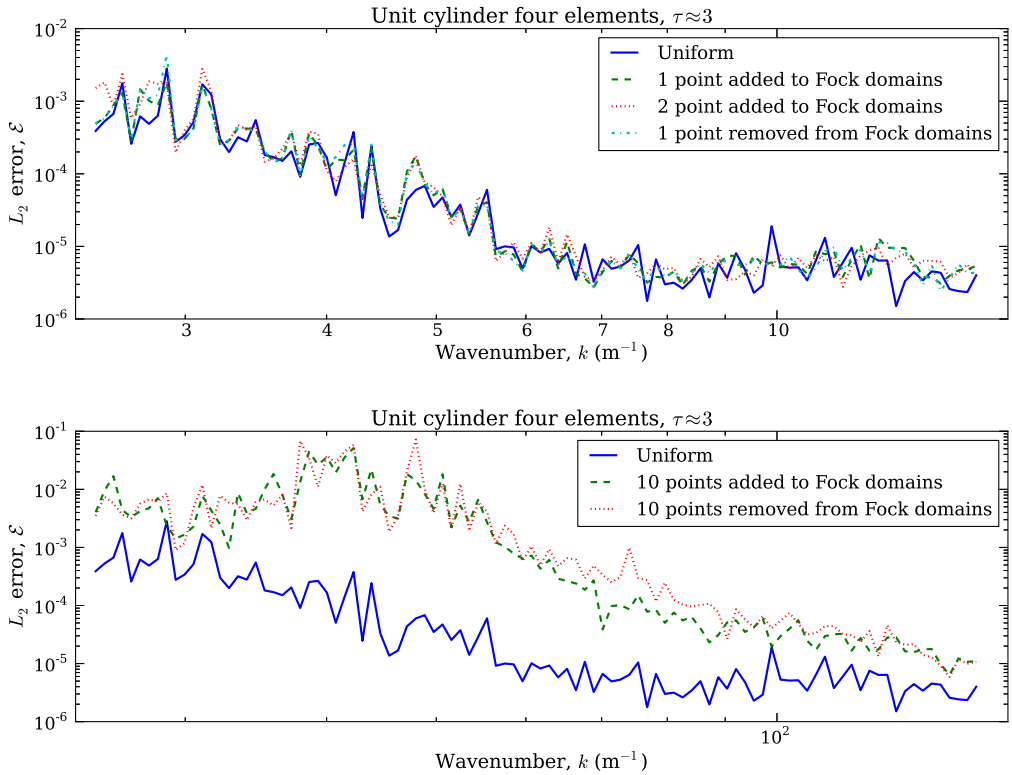

Figure 11. Comparison of collocation strategies with consideration of Fock domain

For asymptotically high wavenumbers, the wave potential in the illuminated zone approaches $2\phi^{/rmI}$; the wave potential in the shadow zone can be considered to be 0. The Fock domain is, therefore, a transition region between these two zones where grazing incidents and high gradients of potential can lead to difficulties in the numerical modelling of the domain.

If there are P collocation points per element, a collocation point can be removed from the illuminated and from the shadow zone and added to the Fock domains. Then the $P-1$ collocation points in the illuminated and shadow zones can be collocated uniformly; similarly, the $P+1$ collocation points in the Fock domains can be collocated uniformly.

Figure 11 shows the errors for simulations, over a range of wavenumbers, when adding or removing points from the Fock domain. In either case, it is clear, that uniformly spaced collocation over the entire boundary provides the best accuracy.

6. CONCLUSIONS

Using the collocation form of the PU-BEM for wave scattering simulations, errors are found to be at a maximum at the element ends. This is due to a lack of continuity, at the element ends, associated with Lagrangian shape functions. It has been shown that trigonometric shape functions increase the continuity at the element ends and, thereby, improve the approximation of potential in such problems. It should be noted that these accuracy gains are not replicable for conventional BEM schemes, i.e. trigonometric shape functions do not improve upon piecewise quadratic approximations unless a plane wave basis is used.

For geometries with geometry blends, the PU-BEM is susceptible to errors at points where different segments blend together. More continuity is required for improve the accuracy in these

DOI: 10.1002/nme

areas. One possible solution is to use non-uniform rational B-splines (NURBS) which would also describe the geometry of circular arcs analytically.

The choice of collocating the boundary integral equation at equally spaced points around the boundary of the scatterer has been shown to be the most effective approach to collocation.

REFERENCES

1. Banaugh RP, Goldsmith W. Diffraction of steady acoustic waves by surfaces of arbitrary shape. *Journal of the Acoustical Society of America* 1963; **35**(10):1590–1601.
2. Copley LG. Fundamental results concerning integral representations in acoustic radiation. *Journal of the Acoustical Society of America* 1968; **44**(1):28–32.
3. Schenck HA. Improved integral formulation for acoustic radiation problems. *Journal of the Acoustical Society of America* July 1968; **44**(1):41–58.
4. Burton AJ, Miller GF. The application of integral equation methods to the numerical solution of some exterior boundary-value problems. *Proceedings of the Royal Society of London. Series A, Mathematical and Physical Sciences* 1971; **323**(1553):201–210.
5. Bettess P. Short-wave scattering: problems and techniques. *Philosophical Transactions of the Royal Society A—Mathematical, Physical & Engineering Sciences* 2004; **362**(1816):421–443.
6. Abboud T, Nédélec JC, Zhou B. Improvement of the integral equation method for high frequency problems. *Third International Conference on Mathematical and Numerical Aspects of Wave Propagation*, SIAM Proceedings Series, SIAM: Philadelphia, 1995; 178–187.
7. Bruno OP, Geuzaine CA, Monro JA, Reitich F. Prescribed error tolerances within fixed computational times for scattering problems of arbitrarily high frequency: the convex case. *Philosophical Transactions of the Royal Society of London Series A—Mathematical, Physical & Engineering Sciences* 2004; **362**(1816):629–645.
8. Langdon S, Chandler-Wilde SN. A wavenumber independent boundary element method for an acoustic scattering problem. *SIAM Journal of Numerical Analysis* 2006; **43**(6):2450–2477.
9. Domínguez V, Graham IG, Smyshlyaev VP. A hybrid numerical-asymptotic boundary integral method for high-frequency acoustic scattering. *Numerische Mathematik* 2007; **106**(3):471–510.
10. Anand A, Boubendir Y, Ecevit F, Reitich F. Analysis of multiple scattering iterations for high-frequency scattering problems. ii: The three-dimensional scalar case. *Numerische Mathematik* 2010; **114**(3):373–427.
11. de la Bourdonnaye A. A microlocal discretization method and its utilization for a scattering problem. *Comptes Rendus de l'Académie des Sciences - Série I* 1994; **318**(4):385–388.
12. Babuška I, Melenk JM. The partition of unity method. *International Journal for Numerical Methods in Engineering* 1997; **40**(4):727–758.
13. Laghrouche O, Bettess P, Astley RJ. Modelling of short wave diffraction problems using approximating systems of plane waves. *International Journal for Numerical Methods in Engineering* 2002; **54**(10):1501–1533.
14. Cessenat O, Després B. Application of an ultra weak variational formulation of elliptic pdes to the two-dimensional helmholtz problem. *SIAM Journal on Numerical Analysis* 1998; **35**(1):255–299.
15. Huttunen T, Monk P, Kaipio JP. Computational aspects of the ultra-weak variational formulation. *Journal of Computational Physics* 2002; **182**(1):27–46.
16. Farhat C, Harari I, Franca LP. The discontinuous enrichment method. *Computer Methods in Applied Mechanics and Engineering* 2001; **190**(48):6455–6479.
17. Ladevèze P, Rouch P, Riou H, Bohineust X. Analysis of medium-frequency vibrations in a frequency range. *Journal of Computational Acoustics* 2003; **11**(2):255–284.
18. Riou H, Ladevèze P, Sourcis B, Faverjon B, Kovalevsky L. An adaptive numerical strategy for the medium-frequency analysis of helmholtz's problem. *Journal of Computational Acoustics* 2012; **20**(1).
19. Bériot H, Perrey-Debain E, Ben Hahar M, Vayssade C. Plane wave basis in galerkin bem for bidimensional wave scattering. *Engineering Analysis with Boundary Elements* 2010; **34**(2):130–143.
20. Perrey-Debain E, Trevelyan J, Bettess P. Plane wave interpolation in direct collocation boundary element method for radiation and wave scattering: numerical aspects and applications. *Journal of Sound and Vibration* 2003; **261**(5):839–858.
21. Trevelyan J, Coates G. On adaptive definition of plane wave basis for wave boundary elements in acoustic scattering: the 2d case. *Computer Modeling in Engineering & Sciences* 2010; **55**(2):147–168.
22. Wrobel LC. *The boundary element method: applications in thermo-fluids and acoustics*, vol. 1. John Wiley & Sons, 2002.
23. Telles JCF. A self-adaptive co-ordinate transformation for efficient numerical evaluation of general boundary element intergrals. *International Journal for Numerical Methods in Engineering* May 1987; **24**(5):959–973.
24. Treeby BE, Pan J. A practical examination of the errors arising in the direct collocation boundary element method for acoustic scattering. *Engineering Analysis with Boundary Elements* 2009; **33**(11):1302–1315.
25. Lachat JC, Watson JO. Effective numerical treatment of boundary integral equations: a formulation for three-dimensional elastostatics. *International Journal for Numerical Methods in Engineering* 1976; **10**(5):991–1005.
26. Seybert AF, Soenarko B, Rizzo FJ, Shippy DJ. An andvanced computational method for radiation and scattering of acoustic waves in three dimensions. *Journal of the Acoustical Society of America* 1985; **77**(2):362–368.
27. Bowman JJ, Senior BA, Uslenghi PLE. *Electromagnetic and acoustic scattering by simple shapes*. Hemisphere: New York, 1987.
28. Linton CM, Evans DV. The interaction of waves with arrays of vertical circular cylinders. *Journal of Fluid Mechanics* 1990; **215**:549–569.

DOI: 10.1002/nme

29. Kondapalli PS, Shippy DJ, Fairweather G. Analysis of acoustic scattering in fluids and solids by the method of fundamental solutions. *Journal of the Acoustical Society of America* 1992; **91**(4):1844–1854.

DOI: 10.1002/nme